Interplay of many-body and single-particle interactions in iridates and rhodates

Natalia B. Perkins,[1] Yuriy Sizyuk,[1] and Peter Wölfle[1,2]

[1]*Department of Physics, University of Wisconsin, Madison, Wisconsin 53706, USA*

[2]*Institute for Condensed Matter Theory and Institute for Nanotechnology, Karlsruhe Institute of Technology, D-76128 Karlsruhe, Germany*

(Received 4 November 2013; revised manuscript received 18 December 2013; published 29 January 2014)

Motivated by recent experiments exploring the spin-orbit-coupled magnetism in 4*d*- and 5*d*-band transition metal oxides, we study magnetic interactions in Ir- and Rh-based compounds. In these systems, the comparable strength of spin-orbit coupling, crystal-field splitting, and Coulomb and Hund's coupling leads to a rich variety of magnetic exchange interactions, leading to new types of ground states. Using a strong coupling approach, we derive effective low-energy superexchange Hamiltonians from the multiorbital Hubbard model by taking full account of the Coulomb and Hund's interactions in the intermediate states. We find that in the presence of strong SOC and lattice distortions the superexchange Hamiltonian contains various kinds of magnetic anisotropies. Here we are primarily interested in the magnetic properties of Sr_2IrO_4 and $Sr_2Ir_{1-x}Rh_xO_4$ compounds. We perform a systematic study of how magnetic interactions in these systems depend on the microscopic parameters and provide a thorough analysis of the resulting magnetic phase diagram. Comparison of our results with experimental data shows good agreement. Finally, we discuss the parameter space in which the spin-flop transition in Sr_2IrO_4, experimentally observed under pressure, can be realized.

DOI: 10.1103/PhysRevB.89.035143 PACS number(s): 75.10.Hk

I. INTRODUCTION

5*d* transition metal oxides, in which orbital degeneracy is accompanied by strong relativistic spin-orbit coupling (SOC), recently received considerable attention, both in experiment and in theory. In these systems the SOC might be comparable to, or even stronger than, the Coulomb and Hund's couplings, and the crystal-field (CF) interactions arising from surrounding oxygen atoms in a nearly octahedral environment. As a result of this unusual hierarchy of on-site interactions, novel quantum and classical states with nontrivial topology and interesting magnetic properties might be stabilized. Fascinating examples of such properties include the Mott insulator ground state of Sr_2IrO_4 [1–15], the potential spin-liquid ground state of $Na_4Ir_3O_8$ [16,17], the anomalous Hall effect in the metallic frustrated pyrochlore $Pr_2Ir_2O_7$ [18–23], nontrivial long-range order, and moment fluctuations in its sister compound $Eu_2Ir_2O_7$ [24,25], unusual magnetic orderings in the honeycomb compounds Na_2IrO_3 and Li_2IrO_3 [26–33], and others.

The main focus of this paper is on developing a theoretical framework which will allow us to understand the microscopic nature of magnetism in the iridium compounds described above. In these systems, the magnetic degrees of freedom are determined by Ir^{4+} ions in $5d^5$ electronic configurations. In contrast to the 3*d*-based oxides, in which a Mott insulating state is established by strong correlations, in iridates with Ir^{4+} ions, the Mott insulating state does not occur without sufficiently strong SOC [2]. This is because the relatively small Coulomb interaction is too weak to open a charge gap for these systems with broad t_{2g} bands at a 5/6 filling factor, such that the systems would be either metals or band insulators. The SOC, however, splits the t_{2g} bands into $\mathbf{J} = 1/2$ and $\mathbf{J} = 3/2$ bands. Four out of five electrons fill the lower $\mathbf{J} = 3/2$ band, and one electron half-fills the $\mathbf{J} = 1/2$ band. Because the $\mathbf{J} = 1/2$ band is relatively narrow, the Coulomb repulsion is sufficient to open a charge gap in the $\mathbf{J} = 1/2$ band and, therefore, a Mott insulating state occurs. In an idealized system without lattice distortions the magnetic degrees of freedom of this insulating state can be described by the $\mathbf{J} = 1/2$ Kramers doublet.

The superexchange Hamiltonians for layered iridium oxides were first derived in the seminal paper by Jackeli and Khalliulin [11]. They found that the superexchange Hamiltonian describing the coupling between $\mathbf{J} = 1/2$ Kramers doublet states on the square lattice, like in Sr_2IrO_4, is predominantly of isotropic Heisenberg superexchange character, while anisotropic terms become relevant only in the presence of lattice distortions. On the honeycomb lattice, like in Na_2IrO_3, the interaction between $\mathbf{J} = 1/2$ Kramers doublet states is highly anisotropic even in the absence of lattice distortions. The anisotropic part of the superexchange coupling has the very peculiar form of the Kitaev interaction. This originates from the competition between SOC and correlation effects, and is nonzero only in the presence of Hund's coupling.

In the present study, we go beyond this work and derive effective superexchange spin Hamiltonians rigorously starting from the exact eigenstates of the single-ion microscopic Hamiltonian. Here, we will be primarily interested in the magnetic properties of the insulating iridium oxides with tetragonal symmetry, in which the Ir ions occupy a square lattice, as in the case of Sr_2IrO_4. While this particular compound is very interesting and has recently attracted much attention [1–8,10–15], the approach proposed here cannot only be easily used to understand the magnetic properties of other iridates belonging to the Ruddlesden-Popper series $Sr_{n+1}Ir_nO_{3n+1}$, but can also be applied to systems with different lattice geometries.

The magnetic properties of Sr_2IrO_4 are very unusual. Below 240 K, Sr_2IrO_4 is a canted antiferromagnet with a small in-plane ferromagnetic moment ($\sim 0.1\mu_B$) [1], which, however, is one to two orders of magnitude larger than that of the analogous canted antiferromagnet La_2CuO_4. Another important experimental finding is that this canting disappears with pressure [8]. These two observations indicate a very strong coupling between magnetic properties and the crystal lattice, which in the presence of SOC can be understood

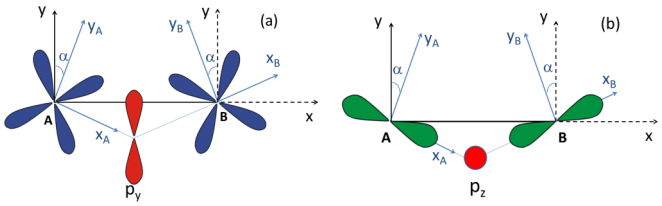

FIG. 1. (Color online) Ir-O-Ir bond in the presence of octahedra rotations in one IrO_2 layer. x and y are the global axes adopted for the intermediate oxygen atoms. $x_{A(B)}$ and $y_{A(B)}$ are local axes on sublattices A and B. (a) Local $\tilde{Z}$ orbital on Ir ion overlaps with p_y oxygen orbital in the global reference frame. (b) Local $\tilde{Y}$ orbital on Ir ion overlaps with p_z oxygen orbital in the global reference frame.

through the coupling of orbital magnetization to the lattice. Consequently, as the orbital magnetic moment contributes to the total magnetic moment of Ir ions, there is a strong dependence of the magnetic degrees on lattice degrees of freedom.

Two types of lattice distortions are present in Sr_2IrO_4 even at ambient pressure: tetragonal distortion and staggered rotation of IrO_6 octahedra (see Fig. 1). The staggered nature of the IrO_6 octahedra rotation leads to a doubling of the unit cell and the formation of a two-sublattice structure. The tetragonal distortion moves the electronic ground state away from the strong SO limit $\mathbf{J} = 1/2$ state by mixing $\mathbf{J} = 1/2$ and $\mathbf{J} = 3/2$ states. Thus in order to understand the magnetism of this system, one needs first to understand the nature of the magnetic degrees of freedom. In our approach we identify the magnetic degrees of freedom by dealing with the exact eigenstates of the full single-ion microscopic Hamiltonian, which includes both SOC and CF interactions.

In this work, we will obtain dependencies of the magnetic interactions on microscopic parameters characterizing the system. In addition, we will study how the properties of Sr_2IrO_4 depend on external pressure [8] and chemical substitution [9,34,35]. In particular, we will discuss the case when iridium is substituted with rhodium [34,35]. Rh substitution, unlike other chemical substitutions, does not change the band filling. However, it varies the SOC, and the Coulomb and Hund's coupling strengths, because on one side the 4d orbitals of Rh ions are less extended, tending to enhance the electronic repulsion and thereby increasing correlation effects, and on the other side, as Rh is a lighter ion, the SOC is smaller. Thus, when the content of Rh increases, the overall balance of on-site interactions changes, and as a result one might expect the appearance of new magnetic phases and doping-driven phase transitions. Although this direction has been recently explored experimentally in a few cases [34,35], it still remains to be investigated theoretically.

The paper is organized as follows. In Sec. II, we introduce the single-ion microscopic model appropriate for the description of the physical properties of the iridates and rhodates, in which five electrons or, equivalently, one hole occupy the threefold degenerate t_{2g} orbitals and experience strong SOC and crystal-field (CF) interactions. We first obtain one-particle eigenstates taking into account only SOC and CF interactions, and then compute two-particle excited eigenstates fully considering correlation effects. In Sec. III we derive an effective superexchange Hamiltonian by integrating out the intermediate oxygen ions and performing a second order perturbation expansion in the hopping parameters around the atomic limit. In Sec. IV, we present our results on the magnetic interactions and show how these interactions depend on various microscopic parameters of the model. We also discuss the application of the results obtained to real compounds. Finally, in Sec. V a summary of the work is presented.

II. SINGLE-ION HAMILTONIAN

A. One-particle eigenstates

In Sr_2IrO_4, the Ir^{+4} ions are sitting inside an oxygen cage forming an octahedron. The octahedral crystal field splits the five 5d orbitals of Ir into a doublet of e_g orbitals at higher energy and into the low-lying threefold degenerate t_{2g} multiplet. In iridates, the energy difference between the e_g and t_{2g} levels is large. Because of this, the five electrons occupy the low lying t_{2g} orbitals and the on-site interactions, such as the SOC, Coulomb and Hund's interactions, and the crystal-field interactions, lowering the symmetry further, can be considered within the t_{2g} manifold only. In this limit, the SOC has to be projected to the t_{2g} manifold, resulting in an effective orbital angular momentum $L = 1$.

It is more convenient to describe the low spin state of the d^5 configuration of Ir^{+4} ions by using the hole description. In the local axes bound to the oxygen octahedron the t_{2g} orbitals of Ir ions are $|X\rangle = |yz\rangle$, $|Y\rangle = |zx\rangle$, and $|Z\rangle = |xy\rangle$. Examples of the lobe structure of the d-wave orbital $|xy\rangle$ of Ir are shown in Fig. 1 (blue lobes). In the absence of interactions, these one-hole states are completely degenerate. The SOC and CF interactions, described by the single-ion Hamiltonian

$$H_{\lambda,\Delta} = \lambda \overrightarrow{S} \cdot \overrightarrow{L} + \Delta L_z^2, \tag{1}$$

give rise to a splitting of the levels according to the symmetry of the underlying lattice. In the tetragonal system, the orbital angular momentum basis is defined by $|L_z = 0\rangle = |Z\rangle$ and $|L_z = \pm 1\rangle = -\frac{1}{\sqrt{2}}(\pm|X\rangle + \imath|Y\rangle)$, where the quantization axis is taken along the tetragonal z axis. In the absence of tetragonal distortion, the energy eigenstates are the angular momentum eigenstates $|J, J_z\rangle$. The full single-particle Hilbert space is, thus, given by a six-component vector $\hat{J} = \{|\frac{1}{2},\frac{1}{2}\rangle, |\frac{1}{2},-\frac{1}{2}\rangle, |\frac{3}{2},\frac{3}{2}\rangle, |\frac{3}{2},\frac{1}{2}\rangle, |\frac{3}{2},-\frac{1}{2}\rangle, |\frac{3}{2},\frac{-3}{2}\rangle\}$. The vector $\hat{J}$ can be expressed in terms of the basis set of t_{2g} orbitals as

$$\hat{J} = \begin{pmatrix} 0 & -\frac{1}{\sqrt{3}} & 0 & -\frac{\imath}{\sqrt{3}} & -\frac{1}{\sqrt{3}} & 0 \\ -\frac{1}{\sqrt{3}} & 0 & \frac{\imath}{\sqrt{3}} & 0 & 0 & \frac{1}{\sqrt{3}} \\ -\frac{1}{\sqrt{2}} & 0 & -\frac{\imath}{\sqrt{2}} & 0 & 0 & 0 \\ 0 & -\frac{1}{\sqrt{6}} & 0 & -\frac{\imath}{\sqrt{6}} & \sqrt{\frac{2}{3}} & 0 \\ \frac{1}{\sqrt{6}} & 0 & -\frac{\imath}{\sqrt{6}} & 0 & 0 & \sqrt{\frac{2}{3}} \\ 0 & \frac{1}{\sqrt{2}} & 0 & -\frac{\imath}{\sqrt{2}} & 0 & 0 \end{pmatrix} \hat{A}_1, \tag{2}$$

where $\hat{A}_1 = \{|X_\uparrow\rangle, |X_\downarrow\rangle, |Y_\uparrow\rangle, |Y_\downarrow\rangle, |Z_\uparrow\rangle, |Z_\downarrow\rangle\}$ is a six-component vector and $\uparrow$, $\downarrow$ indicate spin states. The ground state is a Kramers doublet $|J = \frac{1}{2}, J_z\rangle$ at energy $E_0 = -\lambda$ and the excited state forms a quartet $|J = \frac{3}{2}, J_z\rangle$ at energy $E_1 = \frac{1}{2}\lambda$. However, in Sr_2IrO_4, the tetragonal distortion is present and is not small. It arises because the oxygen octahedra are elongated

along the z axis. In the hole representation, $\Delta = \Delta_{\rm tet} > 0$ and the t_{2g} orbitals are split into a singlet state $|Z\rangle$ with energy $-\Delta$ and a doublet state ($|X\rangle$ and $|Y\rangle$) with energy $\Delta/2$. In the presence of both the tetragonal distortion and the SOC, the eigenfunctions of the Hamiltonian (1) are given by components of a vector $\hat{\Psi} = \{|\Psi_1\rangle,|\Psi_2\rangle,|\Psi_3\rangle,|\Psi_4\rangle,|\Psi_5\rangle,|\Psi_6\rangle\}$, which in terms of t_{2g} orbitals are given by

$$\hat{\Psi} = \hat{M}_\theta^{\rm tet}\hat{A}_1, \tag{3}$$

where

$$\hat{M}_\theta^{\rm tet} = \begin{pmatrix} 0 & \frac{1}{\sqrt{2}}c_\theta & 0 & \frac{\imath}{\sqrt{2}}c_\theta & s_\theta & 0 \\ -\frac{1}{\sqrt{2}}c_\theta & 0 & \frac{\imath}{\sqrt{2}}c_\theta & 0 & 0 & s_\theta \\ -\frac{1}{\sqrt{2}} & 0 & -\frac{\imath}{\sqrt{2}} & 0 & 0 & 0 \\ 0 & -\frac{1}{\sqrt{2}}s_\theta & 0 & -\frac{\imath}{\sqrt{2}}s_\theta & c_\theta & 0 \\ \frac{1}{\sqrt{2}}s_\theta & 0 & -\frac{\imath}{\sqrt{2}}s_\theta & 0 & 0 & c_\theta \\ 0 & -\frac{1}{\sqrt{2}} & 0 & \frac{\imath}{\sqrt{2}} & 0 & 0 \end{pmatrix},$$

where, for shortness, we denote $c_\theta = \cos\theta$ and $s_\theta = \sin\theta$. The angle variable θ is determined by $\tan(2\theta) = 2\sqrt{2}\frac{\lambda}{\lambda-2\Delta}$ and takes care of the competition between the tetragonal distortion and the SOC [11].

The eigenstates of the Hamiltonian (1) are given by the following three doublets: the ground state doublet ($|\Psi_1\rangle$ and $|\Psi_2\rangle$) with energy $E^{(1,2)} = \frac{1}{2}(\Delta - \frac{\lambda}{2}) - \frac{1}{2}\sqrt{2\lambda^2 + (\Delta - \frac{\lambda}{2})^2} = -\frac{\lambda}{\sqrt{2}}\cot\theta$, the intermediate doublet ($|\Psi_4\rangle$ and $|\Psi_5\rangle$) with energy $E^{(4,5)} = \frac{1}{2}(\Delta - \frac{\lambda}{2}) + \frac{1}{2}\sqrt{2\lambda^2 + (\Delta - \frac{\lambda}{2})^2} = \frac{\lambda}{\sqrt{2}}\tan\theta$, and the upper doublet ($|\Psi_3\rangle$ and $|\Psi_6\rangle$) with energy $E^{(3,6)} = \Delta + \frac{\lambda}{2}$. Note that the ground state doublet $|\Psi_1\rangle$ and $|\Psi_2\rangle$ is different from the $|J = \frac{1}{2}, J_z\rangle$ doublet as well as the $L_z = 0$ doublet.

In Sr_2IrO_4, there is also a staggered rotation of neighboring oxygen octahedra by an angle $\pm\alpha$ about the z axis [see Figs. 1(a) and 1(b)] leading to the formation of a two-sublattice structure. We denote these two sublattices as A and B. Because the crystal-field interaction on Ir $5d$ orbitals is diagonal only in the local cubic axes bound to the oxygen octahedron, in the presence of the octahedra rotations, atomic states on sublattices A and B have to be defined in the local basis. Then, the states on sublattices A and B are given by

$$\hat{\Psi}_A = \hat{M}_\theta^{\rm tet}\begin{pmatrix} |\tilde{X}_\uparrow e^{-\frac{\imath\alpha}{2}}\rangle \\ |\tilde{X}_\downarrow e^{\frac{\imath\alpha}{2}}\rangle \\ |\tilde{Y}_\uparrow e^{-\frac{\imath\alpha}{2}}\rangle \\ |\tilde{Y}_\downarrow e^{\frac{\imath\alpha}{2}}\rangle \\ |\tilde{Z}_\uparrow e^{-\frac{\imath\alpha}{2}}\rangle \\ |\tilde{Z}_\downarrow e^{\frac{\imath\alpha}{2}}\rangle \end{pmatrix} \tag{4}$$

and

$$\hat{\Psi}_B = \hat{M}_\theta^{\rm tet}\begin{pmatrix} |\tilde{X}_\uparrow e^{\frac{\imath\alpha}{2}}\rangle \\ |\tilde{X}_\downarrow e^{-\frac{\imath\alpha}{2}}\rangle \\ |\tilde{Y}_\uparrow e^{\frac{\imath\alpha}{2}}\rangle \\ |\tilde{Y}_\downarrow e^{-\frac{\imath\alpha}{2}}\rangle \\ |\tilde{Z}_\uparrow e^{\frac{\imath\alpha}{2}}\rangle \\ |\tilde{Z}_\downarrow e^{-\frac{\imath\alpha}{2}}\rangle \end{pmatrix}, \tag{5}$$

where the phase factors $e^{\pm\frac{\imath\alpha}{2}}$ appear after the projection of the spin states onto the local reference frame. Initially the spin states are defined in the global reference frame.

B. Two-hole states in the presence of interactions, spin-orbit coupling, and tetragonal distortion

The many-body part of the single-ion Hamiltonian is given by the three-band Hubbard Hamiltonian of the form

$$\begin{aligned} H_{\rm int} = {} & U_1\sum_{i,\alpha} n_{i\alpha\uparrow}n_{i\alpha\downarrow} + \frac{1}{2}(U_2 - J_H)\sum_{i,\sigma,\alpha\neq\alpha'} n_{i\alpha\sigma}n_{i\alpha'\sigma} \\ & + U_2\sum_{i,\alpha\neq\alpha'} n_{i\alpha\uparrow}n_{i\alpha'\downarrow} + J_H\sum_{i,\alpha\neq\alpha'} d^\dagger_{i\alpha\uparrow}d^\dagger_{i\alpha\downarrow}d_{i\alpha'\downarrow}d_{i\alpha'\uparrow} \\ & - J_H\sum_{i,\alpha\neq\alpha'} d^\dagger_{i\alpha\uparrow}d_{i\alpha\downarrow}d^\dagger_{i\alpha'\downarrow}d_{i\alpha'\uparrow}, \end{aligned} \tag{6}$$

where U_1 and U_2 are the Coulomb repulsion among electrons in the same and in different t_{2g} orbitals, respectively, and J_H is the Hund's coupling constant. Due to the cubic symmetry, the relation $U_1 = U_2 + 2J_H$ holds. The annihilation and creation electron operators, $d_{i\alpha\sigma}$ and $d^\dagger_{i\alpha\sigma}$, refer to Ir orbitals at site i, of type α (X, Y, or Z), and with spin $\sigma = \uparrow, \downarrow$ and $n_{i\alpha\sigma} = d^\dagger_{i\alpha\sigma}d_{i\alpha\sigma}$. In order to obtain $H_{\rm int}$ in the hole picture, we substitute $d^\dagger_{\alpha\sigma} \to a_{\alpha\sigma}$ and $n_{\alpha\sigma} \to 1 - h_{\alpha\sigma}$, where $h_{\alpha\sigma} = a^\dagger_{\alpha\sigma}a_{\alpha\sigma}$, and $a^\dagger_{\alpha\sigma}$ and $a_{\alpha\sigma}$ are the hole creation and annihilation operators.

We first compute energy eigenvalues of $H_{\rm int}$. We consider ground states with one hole on the Ir ion and excited states, in which the Ir ion can have two holes or no holes. The corresponding energies are

$$\begin{aligned} E_{1h} &= 10U_2, \\ E_{0h} &= 15U_2, \\ E^{(1)}_{2h} &= 6U_2 - J_H, \\ E^{(0)}_{2h} &= 6U_2 + J_H, \\ E^{(00)}_{2h} &= 6U_2 + 4J_H. \end{aligned} \tag{7}$$

There are $6 \times 5/2 = 15$ partly degenerate two-hole states: six spin singlets and three triplets. Let the vector $|\mathcal{I}\rangle = |\mathcal{I}; n\rangle$ denote the two-hole eigenstates. It is convenient to represent them using the cubic orbital basis,

$$\hat{\mathcal{I}} = \hat{\mathcal{M}}_2\hat{A}_2, \tag{8}$$

where

$$\begin{aligned} \hat{A}_2 = \{ & X_\uparrow X_\downarrow, X_\uparrow Y_\uparrow, X_\uparrow Y_\downarrow, X_\uparrow Z_\uparrow, X_\uparrow Z_\downarrow, X_\downarrow Y_\uparrow, X_\downarrow Y_\downarrow, \\ & X_\downarrow Z_\uparrow, X_\downarrow Z_\downarrow, Y_\uparrow Y_\downarrow, Y_\uparrow Z_\uparrow, Y_\uparrow Z_\downarrow, Y_\downarrow Z_\uparrow, Y_\downarrow Z_\downarrow, Z_\uparrow Z_\downarrow\} \end{aligned}$$

is the two-hole orbital basis and the transformation matrix $\hat{\mathcal{M}}_2$ can be easily obtained. Explicitly, vector $\hat{\mathcal{I}}$ consists of the following elements.

(i) Symmetric state with singlet pairs on the same orbital $S = 0, \alpha = \alpha'$,

$$|\mathcal{I}; 1\rangle = \frac{1}{\sqrt{3}}(a^\dagger_{X\downarrow}a^\dagger_{X\uparrow} + a^\dagger_{Y\downarrow}a^\dagger_{Y\uparrow} + a^\dagger_{Z\downarrow}a^\dagger_{Z\uparrow})|{\rm vac}\rangle,$$

with energy equal to $E_1 = E^{(00)}_{2h} = 6U_2 + 4J_H = E_d$.

(ii) Two degenerate antisymmetric states with singlet pairs on the same orbital $S = 0, \alpha = \alpha'$,

$$|\mathcal{I}; 2\rangle = \frac{1}{\sqrt{2}}(a^\dagger_{X\downarrow}a^\dagger_{X\uparrow} - a^\dagger_{Y\downarrow}a^\dagger_{Y\uparrow})|{\rm vac}\rangle$$

$$|\mathcal{I};3\rangle = \frac{1}{\sqrt{6}}(a^\dagger_{X\downarrow}a^\dagger_{X\uparrow} + a^\dagger_{Y\downarrow}a^\dagger_{Y\uparrow} - 2a^\dagger_{Z\downarrow}a^\dagger_{Z\uparrow})|\text{vac}\rangle,$$

with energies equal to $E_{2,3} = E^{(0)}_{2h} = 6U_2 + J_H = E_s$.

(iii) Three states with singlet pairs on different orbitals $S = 0, \alpha \neq \alpha'$,

$$\begin{aligned}
|\mathcal{I};4\rangle &= \frac{1}{\sqrt{2}}(a^\dagger_{X\downarrow}a^\dagger_{Y\uparrow} - a^\dagger_{X\uparrow}a^\dagger_{Y\downarrow})|\text{vac}\rangle,\\
|\mathcal{I};5\rangle &= \frac{1}{\sqrt{2}}(a^\dagger_{Y\downarrow}a^\dagger_{Z\uparrow} - a^\dagger_{Z\uparrow}a^\dagger_{Y\downarrow})|\text{vac}\rangle,\\
|\mathcal{I};6\rangle &= \frac{1}{\sqrt{2}}(a^\dagger_{Z\downarrow}a^\dagger_{X\uparrow} - a^\dagger_{X\uparrow}a^\dagger_{Z\downarrow})|\text{vac}\rangle,
\end{aligned}$$

with $E_{4,5,6} = E^{(0)}_{2h} = 6U_2 + J_H = E_s$.

(iv) Nine states with triplet pairs on different orbitals $S = 1, \alpha \neq \alpha'$,

$$\begin{aligned}
|\mathcal{I};7\rangle &= \frac{1}{\sqrt{2}}(a^\dagger_{X\downarrow}a^\dagger_{Y\uparrow} + a^\dagger_{X\uparrow}a^\dagger_{Y\downarrow})|\text{vac}\rangle,\\
|\mathcal{I};8\rangle &= a^\dagger_{X\uparrow}a^\dagger_{Y\uparrow}|\text{vac}\rangle,\\
|\mathcal{I};9\rangle &= a^\dagger_{X\downarrow}a^\dagger_{Y\downarrow}|\text{vac}\rangle,\\
|\mathcal{I};10\rangle &= \frac{1}{\sqrt{2}}(a^\dagger_{Y\downarrow}a^\dagger_{Z\uparrow} + a^\dagger_{Y\uparrow}a^\dagger_{Z\downarrow})|\text{vac}\rangle,\\
|\mathcal{I};11\rangle &= a^\dagger_{Y\uparrow}a^\dagger_{Z\uparrow}|\text{vac}\rangle,\\
|\mathcal{I};12\rangle &= a^\dagger_{Y\downarrow}a^\dagger_{Z\downarrow}|\text{vac}\rangle,\\
|\mathcal{I};13\rangle &= \frac{1}{\sqrt{2}}(a^\dagger_{Z\downarrow}a^\dagger_{X\uparrow} + a^\dagger_{Z\uparrow}a^\dagger_{X\downarrow})|\text{vac}\rangle,\\
|\mathcal{I};14\rangle &= a^\dagger_{Z\uparrow}a^\dagger_{X\uparrow}|\text{vac}\rangle,\\
|\mathcal{I};15\rangle &= a^\dagger_{Z\downarrow}a^\dagger_{X\downarrow}|\text{vac}\rangle,
\end{aligned}$$

with energies $E_{7,\ldots,15} = E^{(1)}_4 = 6U_2 - J_H = E_t$. This gives three different excitation energies:

$$\begin{aligned}
\Delta E_1 &= E_d + E_{0h} - 2E_{1h} = U_2 + 4J_H,\\
\Delta E_2 &= E_s + E_{0h} - 2E_{1h} = U_2 + J_H,\\
\Delta E_3 &= E_t + E_{0h} - 2E_{1h} = U_2 - J_H.
\end{aligned} \tag{9}$$

In the presence of the SOC and lattice distortions, the two-hole states $|\mathcal{I};n\rangle$ are mixed, and the true two-hole eigenstates are obtained by diagonalization of the full on-site Hamiltonian,

$$H_{\text{int}+\lambda,\Delta} = H_{\text{int}} + H_{\lambda,\Delta}. \tag{10}$$

To this end, it is convenient first to represent the $|\mathcal{I};n\rangle$ states in terms of the eigenstates of $H_{\lambda,\Delta}$. The two-hole eigenstates of the SOC part of the Hamiltonian are simply given by product states $|\mathcal{J},\mu\rangle \equiv |J_1, J_{1z}; J_2, J_{2z}\rangle$:

$$\begin{aligned}
|\mathcal{J},1\rangle &\equiv \left|\tfrac{1}{2},\tfrac{1}{2};\tfrac{3}{2},\tfrac{3}{2}\right\rangle,\\
|\mathcal{J},2\rangle &\equiv \left|\tfrac{1}{2},-\tfrac{1}{2};\tfrac{3}{2},\tfrac{3}{2}\right\rangle,\\
|\mathcal{J},3\rangle &\equiv \left|\tfrac{1}{2},\tfrac{1}{2};\tfrac{3}{2},\tfrac{1}{2}\right\rangle,\\
|\mathcal{J},4\rangle &\equiv \left|\tfrac{1}{2},-\tfrac{1}{2};\tfrac{3}{2},\tfrac{1}{2}\right\rangle,\\
|\mathcal{J},5\rangle &\equiv \left|\tfrac{1}{2},\tfrac{1}{2};\tfrac{3}{2},-\tfrac{1}{2}\right\rangle,\\
|\mathcal{J},6\rangle &\equiv \left|\tfrac{1}{2},-\tfrac{1}{2};\tfrac{3}{2},-\tfrac{1}{2}\right\rangle,\\
|\mathcal{J},7\rangle &\equiv \left|\tfrac{1}{2},\tfrac{1}{2};\tfrac{3}{2},-\tfrac{3}{2}\right\rangle,\\
|\mathcal{J},8\rangle &\equiv \left|\tfrac{1}{2},-\tfrac{1}{2};\tfrac{3}{2},-\tfrac{3}{2}\right\rangle,\\
|\mathcal{J},9\rangle &\equiv \left|\tfrac{1}{2},\tfrac{1}{2};\tfrac{1}{2},-\tfrac{1}{2}\right\rangle,\\
|\mathcal{J},10\rangle &\equiv \left|\tfrac{3}{2},\tfrac{1}{2};\tfrac{3}{2},\tfrac{3}{2}\right\rangle,\\
|\mathcal{J},11\rangle &\equiv \left|\tfrac{3}{2},-\tfrac{1}{2};\tfrac{3}{2},\tfrac{3}{2}\right\rangle,\\
|\mathcal{J},12\rangle &\equiv \left|\tfrac{3}{2},-\tfrac{3}{2};\tfrac{3}{2},\tfrac{3}{2}\right\rangle,\\
|\mathcal{J},13\rangle &\equiv \left|\tfrac{3}{2},-\tfrac{1}{2};\tfrac{3}{2},\tfrac{1}{2}\right\rangle,\\
|\mathcal{J},14\rangle &\equiv \left|\tfrac{3}{2},-\tfrac{3}{2};\tfrac{3}{2},\tfrac{1}{2}\right\rangle,\\
|\mathcal{J},15\rangle &\equiv \left|\tfrac{3}{2},-\tfrac{3}{2};\tfrac{3}{2},-\tfrac{1}{2}\right\rangle.
\end{aligned} \tag{11}$$

In short, these states can be written as

$$|\mathcal{J},\mu\rangle = \sum_{\gamma_1,\gamma_2=1}^{6} m^{\mu}_{\gamma_1,\gamma_2} b^\dagger_{\gamma_1} b^\dagger_{\gamma_2}|\text{vac}\rangle, \tag{12}$$

where $\mu = 1,\ldots,15$ refers to the component of the vector $\hat{\mathcal{J}}$ and $b^\dagger_\gamma$ is an operator creating a hole of the type $\gamma = 1,\ldots,6$, which refers to the component of the single-hole vector $\hat{J}$. The tensor $\hat{m}$ has the following nonzero elements:

$$\begin{aligned}
&m^1_{1,3} = m^2_{2,3} = m^3_{1,4} = m^4_{2,4} = m^5_{1,5}\\
&= m^6_{2,5} = m^7_{1,6} = m^8_{2,6} = m^9_{1,2} = m^{10}_{4,3}\\
&= m^{11}_{5,3} = m^{12}_{6,3} = m^{13}_{5,4} = m^{14}_{6,4} = m^{15}_{6,5} = 1.
\end{aligned}$$

If, in addition to the SOC, the lattice distortion is present, the two-hole states $|\tilde{\mathcal{J}},\mu\rangle$ are given by the products of two $|\Psi_n\rangle$ states. The explicit form of the vector $|\tilde{\mathcal{J}},\mu\rangle$ can be easily obtained from Eq. (11) by the following substitution:

$$\begin{aligned}
\left|\tfrac{1}{2},\tfrac{1}{2}\right\rangle &\to |\Psi_1\rangle,\\
\left|\tfrac{1}{2},-\tfrac{1}{2}\right\rangle &\to |\Psi_2\rangle,\\
\left|\tfrac{3}{2},\tfrac{3}{2}\right\rangle &\to |\Psi_3\rangle,\\
\left|\tfrac{3}{2},\tfrac{1}{2}\right\rangle &\to |\Psi_4\rangle,\\
\left|\tfrac{3}{2},-\tfrac{1}{2}\right\rangle &\to |\Psi_5\rangle,\\
\left|\tfrac{3}{2},-\tfrac{3}{2}\right\rangle &\to |\Psi_6\rangle.
\end{aligned} \tag{13}$$

The complete Hamiltonian matrix has the same block diagonal structure in the space of states $|\mathcal{J},\mu\rangle$ and $|\tilde{\mathcal{J}},\mu\rangle$. Therefore, below we will omit the tilde sign and use notations $|\mathcal{J},\mu\rangle$ in a general sense.

In the $|\mathcal{J},\mu\rangle$ basis, the Hamiltonian matrix is given by

$$\langle\mathcal{J},\mu'|H_{\text{int}+\lambda,\Delta}|\mathcal{J},\mu\rangle = \epsilon_\mu\delta_{\mu'\mu} + \sum_{n=1}^{15} E_n\langle\mathcal{J},\mu'|\mathcal{I},n\rangle\langle\mathcal{I},n|\mathcal{J},\mu\rangle, \quad (14)$$

where ϵ_μ is the energy of the $|\mathcal{J},\mu\rangle$ state and the $\langle\mathcal{J},\mu|\mathcal{I},n\rangle$ denote components of the overlap matrix. The diagonalization of (14) gives energy eigenstates of the full Hamiltonian,

$$|D,\xi\rangle = \sum_{\mu=1}^{15} c_{\xi\mu}|\mathcal{J},\mu\rangle, \quad (15)$$

where $\xi = 1,\ldots,15$ and $c_{\xi\mu}$ denote the eigenvectors. We denote the energy eigenvalues as E_ξ. The block structure of the Hamiltonian matrix is given in Appendix A. As a final remark, we also note that in the limit $J_H = 0$ and $\Delta = 0$, the Hamiltonian matrix (14) is diagonal with $E_1 = \cdots = E_8 = -\lambda/2 + 6U_2$, $E_9 = -2\lambda + 6U_2$, and $E_{10} = \cdots = E_{15} = \lambda + 6U_2$.

III. DERIVATION OF THE SUPEREXCHANGE HAMILTONIAN

In systems with tetragonal symmetry, the Ir-O-Ir bonds are close to 180°. In these systems, in general, the contribution to the superexchange coupling from direct Ir-Ir hopping may be neglected because the Ir ions are quite far from each other. The dominant contribution to the superexchange is from the hopping via intermediate oxygen ions, so-called oxygen-assisted hopping. Because intermediate states with two holes on the oxygen ion have high energy and, thus, can be neglected, we may integrate out the oxygen degrees of freedom to obtain an effective oxygen-assisted hopping between Ir $5d$ states. Then applying a second order perturbation theory expansion in the effective hopping parameters, we obtain a superexchange Hamiltonian in the following form:

$$H_{\text{ex},n,n'} = \sum_\xi \frac{1}{\epsilon_\xi} P H_{t,n,n'} Q_{\xi,n'} H_{t,n',n} P, \quad (16)$$

where

$$P = \sum_{\sigma_n=\pm1} |1/2,\sigma_n/2;n\rangle\langle n;1/2,\sigma_n/2| \quad (17)$$

is the projection operator onto the ground states with one hole at site n. The projection operators onto two-hole intermediate states $|D,\xi;n'\rangle$ with excitation energy ϵ_ξ at site n' are then given by

$$Q_{\xi,n'} = |D,\xi;n'\rangle\langle n';D,\xi| = D^\dagger_{\xi,n'} D_{\xi,n'}. \quad (18)$$

The excitation energies of the intermediate states are $\epsilon_\xi = E_{0h} + E_\xi - 2E_{1h}$.

The connection between the Kramers doublet ground states at site n ($\gamma = 1,2$) and the full manifold of states at site n' ($\gamma' = 1,2,\ldots,6$) is given by the projected hopping term:

$$P H_{t,n,n'} = \sum_{\gamma=1}^{2}\sum_{\gamma'=1}^{6} T^{\gamma,\gamma'}_{n,n'} b^\dagger_{n,\gamma} b_{n',\gamma'}, \quad (19)$$

where the elements of the matrix $T^{\gamma,\gamma'}_{n,n'}$ describe an overlap between $|J,J_z\rangle$ or $|\Psi_\gamma\rangle$ states in the absence or in the presence of the tetragonal distortion, respectively. Explicitly, these matrices are derived in Appendix B. Next, we apply $P H_{t,n,n'}$ to the $D^\dagger_{\xi,n'}$ state and obtain

$$\begin{aligned} &P H_{t,n,n'} D^\dagger_{\xi,n'} \\ &= \sum_{\gamma=1}^{2}\sum_{\gamma'=1}^{6} T^{\gamma,\gamma'}_{n,n'} b^\dagger_{n,\gamma} b_{n',\gamma'} \sum_{\nu=1}^{15}\sum_{\gamma_1,\gamma_2=1}^{6} c_{\xi,\nu} m^\nu_{\gamma_1\gamma_2} b^\dagger_{n',\gamma_1} b^\dagger_{n',\gamma_2} \\ &= \sum_{\gamma,\gamma'=1}^{2}\sum_{\gamma_1=1}^{6}\sum_{\nu=1}^{15} T^{\gamma,\gamma_1}_{n,n'} c_{\xi,\nu}\left(m^\nu_{\gamma_1\gamma'} - m^\nu_{\gamma'\gamma_1}\right) b^\dagger_{n,\gamma} b^\dagger_{n',\gamma'}. \end{aligned} \quad (20)$$

Here the terms with $b^\dagger_{n',\gamma_1} b^\dagger_{n',\gamma_2}$ for $\gamma_1,\gamma_2 > 2$ are projected out by the operator $P_{n'}$. Finally, using the following relation:

$$P H_t Q_{\xi,n'} H_t P = [P H_t D^\dagger_{\xi,n'}][P H_t D^\dagger_{\xi,n'}]^\dagger, \quad (21)$$

where

$$P H_{t,n,n'} D^\dagger_{\xi,n'} = \sum_{\sigma,\sigma'=\pm1} A^\xi_{\sigma,\sigma'} b^\dagger_{n,\sigma} b^\dagger_{n',\sigma'}, \quad (22)$$

with

$$A^\xi_{n,n';\sigma,\sigma'} = \sum_{\gamma_1=1}^{6}\sum_{\nu=1}^{15} T^{\sigma,\gamma_1}_{n,n'} c_{\xi,\nu}\left(m^\nu_{\gamma_1\sigma'} - m^\nu_{\sigma'\gamma_1}\right), \quad (23)$$

we write the exchange Hamiltonian as

$$H_{ex,n,n'} = \sum_{\sigma,\sigma'=1}^{2}\sum_{\sigma_1,\sigma_1'=1}^{2}\sum_{\xi=1}^{15} \times\frac{1}{\epsilon_\xi}\left\{A^\xi_{n,n';\sigma,\sigma'} b^\dagger_{n,\sigma} b^\dagger_{n',\sigma'} A^\xi_{n',n;\sigma_1',\sigma_1} b_{n',\sigma_1'} b_{n,\sigma_1}\right\}. \quad (24)$$

We note that $A^\xi_{n',n;\sigma',\sigma} = (A^\xi_{n,n';\sigma,\sigma'})^*$. In the following, in order to shorten notations, we omit the site indices denoting $A^\xi_{n,n';\sigma,\sigma'} \equiv A^\xi_{\sigma,\sigma'}$ and $A^\xi_{n',n;\sigma',\sigma} \equiv (A^\xi_{\sigma,\sigma'})^*$. We also observe that $\sum_\xi \frac{1}{\epsilon_\xi} A^\xi_{\sigma,\sigma} A^\xi_{\sigma_1,-\sigma_1} = 0$, since $A^\xi_{\sigma,\sigma}$ and $A^\xi_{\sigma_1,-\sigma_1}$ connect different groups of states $|D,\xi\rangle$ and are therefore "orthogonal." Defining operators $B_{n\sigma\sigma'} = b^\dagger_{n,\sigma} b_{n,\sigma'}$, we may write the superexchange Hamiltonian (24) in the form

$$\begin{aligned} H_{\text{ex},n,n'} = &\sum_{\xi=1}^{15}\frac{1}{\epsilon_\xi} \\ &\times\{A^\xi_{\uparrow\uparrow}(A^\xi_{\uparrow\uparrow})^*(B_{n\uparrow\uparrow}B_{n'\uparrow\uparrow} + B_{n\downarrow\downarrow}B_{n'\downarrow\downarrow}) \\ &+ A^\xi_{\uparrow\downarrow}(A^\xi_{\uparrow\downarrow})^*(B_{n\uparrow\uparrow}B_{n'\downarrow\downarrow} + B_{n\downarrow\downarrow}B_{n'\uparrow\uparrow}) \\ &+ A^\xi_{\uparrow\downarrow}(A^\xi_{\downarrow\uparrow})^*(B_{n\uparrow\downarrow}B_{n'\downarrow\uparrow} + B_{n\downarrow\uparrow}B_{n'\uparrow\downarrow}) \\ &+ A^\xi_{\uparrow\uparrow}(A^\xi_{\downarrow\downarrow})^*(B_{n\uparrow\downarrow}B_{n'\uparrow\downarrow} + B_{n\downarrow\uparrow}B_{n'\downarrow\uparrow})\}. \end{aligned} \quad (25)$$

Next, we introduce pseudospin operators $S^\alpha_n = \frac{1}{2}\sum_{\sigma,\sigma'=\pm1}\tau^\alpha_{\sigma,\sigma'} b^\dagger_{\sigma,n} b_{\sigma',n}$ with the Pauli matrices $\tau^\alpha_{\sigma,\sigma'}, \alpha = x,y,z$ and $\rho_n = \sum_{\sigma=\pm1} b^\dagger_{\sigma,n} b_{\sigma,n}$ and express

operators $B_{n\sigma\sigma'}$ in terms of pseudospin operators as

$$\begin{aligned} B_{n\uparrow\uparrow} &= S^z_n + \rho_n, \\ B_{n\downarrow\downarrow} &= -S^z_n + \rho_n, \\ B_{n\uparrow\downarrow} &= S^+_n, \\ B_{n\downarrow\uparrow} &= S^-_n. \end{aligned} \tag{26}$$

This allows us to write the superexchange Hamiltonian (25) on the bond n,n' in terms of the magnetic degrees of freedom of Ir^{4+} as

$$\begin{aligned} H_{\mathrm{ex},n,n'} = {} & J_z S^z_n S^z_{n'} + J_x S^x_n S^x_{n'} + J_y S^y_n S^y_{n'} \\ & - D\left(S^x_n S^y_{n'} - S^y_n S^x_{n'}\right) + W\rho_n\rho_{n'}, \end{aligned} \tag{27}$$

where the coupling constants are given by the following expressions:

$$\begin{aligned} J_z = -2\sum_\xi \frac{1}{\epsilon_\xi}[& A^\xi_{\uparrow\uparrow}(A^\xi_{\uparrow\uparrow})^* + A^\xi_{\downarrow\downarrow}(A^\xi_{\downarrow\downarrow})^* \\ & - A^\xi_{\uparrow\downarrow}(A^\xi_{\uparrow\downarrow})^* - A^\xi_{\downarrow\uparrow}(A^\xi_{\downarrow\uparrow})^*], \end{aligned} \tag{28}$$

$$\begin{aligned} J_x = -2\sum_\xi \frac{1}{\epsilon_\xi}[& A^\xi_{\uparrow\uparrow}(A^\xi_{\downarrow\downarrow})^* + A^\xi_{\downarrow\downarrow}(A^\xi_{\uparrow\uparrow})^* \\ & + A^\xi_{\uparrow\downarrow}(A^\xi_{\downarrow\uparrow})^* + A^\xi_{\downarrow\uparrow}(A^\xi_{\uparrow\downarrow})^*], \end{aligned} \tag{29}$$

$$\begin{aligned} J_y = 2\sum_\xi \frac{1}{\epsilon_\xi}[& A^\xi_{\uparrow\uparrow}(A^\xi_{\downarrow\downarrow})^* + A^\xi_{\downarrow\downarrow}(A^\xi_{\uparrow\uparrow})^* \\ & - A^\xi_{\uparrow\downarrow}(A^\xi_{\downarrow\uparrow})^* - A^\xi_{\downarrow\uparrow}(A^\xi_{\uparrow\downarrow})^*], \end{aligned} \tag{30}$$

$$D = 2\imath\sum_\xi \frac{1}{\epsilon_\xi}[A^\xi_{\uparrow\downarrow}(A^\xi_{\downarrow\uparrow})^* - A^\xi_{\downarrow\uparrow}(A^\xi_{\uparrow\downarrow})^*], \tag{31}$$

$$\begin{aligned} W = -2\sum_\xi \frac{1}{\epsilon_\xi}[& A^\xi_{\uparrow\uparrow}(A^\xi_{\uparrow\uparrow})^* + A^\xi_{\downarrow\downarrow}(A^\xi_{\downarrow\downarrow})^* \\ & + A^\xi_{\uparrow\downarrow}(A^\xi_{\uparrow\downarrow})^* + A^\xi_{\downarrow\uparrow}(A^\xi_{\downarrow\uparrow})^*]. \end{aligned} \tag{32}$$

The last interaction term W gives a constant energy shift and we will omit it. It is also convenient to rewrite the remaining terms introducing the following notations: $\delta J_z = J_z - J_y$, $\delta J_{xy} = J_x - J_y$ on x bond and $\delta J_z = J_z - J_x$, $\delta J_{xy} = J_y - J_x$ on y bond. Then, $H_{\mathrm{ex},n,n'}$ can be written as

$$\begin{aligned} H_{\mathrm{ex},n,n'} = {} & J\mathbf{S}_n\mathbf{S}_{n'} - D\left(S^x_n S^y_{n'} - S^y_n S^x_{n'}\right) \\ & + \delta J_z S^z_n S^z_{n'} + \delta J_{xy}(\mathbf{S}_n\cdot\mathbf{r}_{n,n'})(\mathbf{S}_{n'}\cdot\mathbf{r}_{n,n'}), \end{aligned} \tag{33}$$

where $\mathbf{r}_{n,n'}$ is the unit vector along the n,n' bond. In this form the nature of interactions between pseudospin moments S is more clear. The first term describes the Heisenberg isotropic interaction with a coupling constant $J = J_y$ on the x bond. We note that for any possible set of microscopic parameters, the isotropic exchange is the dominant exchange and has AFM nature. The second term is a Dzyaloshinsky-Moriya (DM) interaction with a coupling constant D, which leads to a spin canting in the xy plane proportional to the ratio D/J. The third term describes an additional Ising-like interaction of z components of spins. $\delta J_z > 0$ favors AFM ordering of spins along the z axis and works as an easy axis anisotropy. $\delta J_z < 0$ supports FM ordering of spins along the z axis and works as an easy plane anisotropy. The last term is a pseudodipolar interaction. Finally, the total superexchange Hamiltonian is given by

$$H = \sum_{\langle n,n'\rangle} H_{\mathrm{ex},n,n'}, \tag{34}$$

where summation is over all bonds of the lattice.

IV. RESULTS AND DISCUSSIONS

A. Application to Sr_2IrO_4

Below we present our results on how the exchange coupling constants J_x, J_y, J_z and anisotropic couplings $\delta J_{xy}, \delta J_z$ and D depend on the microscopic parameters of the system. We first note that the main role of the Coulomb repulsion is to determine the overall energy scale for the couplings. In all computations we take $U_2 = 1.8$ eV, which lays inside the range of values, 1.5–2.5 eV, characteristic for iridates [13,15]. We will mostly set the SOC constant to be equal to $\lambda = 0.4$ eV—the value associated with Ir ions in the literature; however, we will also consider the smaller value $\lambda = 0.22$ eV, which was suggested in the experimental work by Haskel *et al.* [8].

Sr_2IrO_4 is also characterized by various structural distortions, the most important of which are the tetragonal distortion and rotations of the oxygen octahedra. Both of them are present even at ambient pressure. In calculations we either consider the tetragonal distortion and the angle of rotation to be equal to $\Delta = 0.15$ eV and $\alpha = 0.2$ rad, respectively, or we study how the exchange parameters depend on these quantities.

Finally, we consider the hopping parameter between Ir ions to be equal to $t_{\mathrm{eff}} = 0.13$ eV, which is slightly lower than the values 0.2–0.3 eV suggested by *ab initio* calculations. These values of hoppings give too large values of exchange couplings if all other parameters are set as we described above. We believe, however, that hopping parameters obtained within density functional theory are often reduced when correlations are taken into account.

The effect of Hund's coupling. In Fig. 2(a) we plot the anisotropic couplings $\delta J_{xy}, \delta J_z$ and the DM interaction constant D as functions of Hund's coupling, J_H, in the absence of octahedral rotations, $\alpha = 0$. In this case, the components of the vectors $A^\xi_{\sigma,\sigma'}$ (23) satisfy the following conditions:

$$\begin{aligned} \sum_\xi \frac{1}{\epsilon_\xi}(A^\xi_{\uparrow\uparrow})^2 &= \sum_\xi \frac{1}{\epsilon_\xi}(A^\xi_{\downarrow\downarrow})^2, \\ \sum_\xi \frac{1}{\epsilon_\xi}(A^\xi_{\uparrow\downarrow})^2 &= \sum_\xi \frac{1}{\epsilon_\xi}(A^\xi_{\downarrow\uparrow})^2. \end{aligned} \tag{35}$$

This symmetry reflects the fact that in the absence of the octahedra rotations there is no spin dependent hopping and, consequently, no DM interaction. The anisotropic terms δJ_z and δJ_{xy} are also zero at $\alpha = 0$ and $J_H = 0$ eV, but they acquire finite values at $J_H \neq 0$. We note that the Ising-like interaction, $\delta J_z < 0$, makes the xy plane the pseudospin's easy plane.

In Fig. 2(b) we plot the exchange couplings J_x, J_y, J_z as functions of the Hund's coupling. On the x bond, the

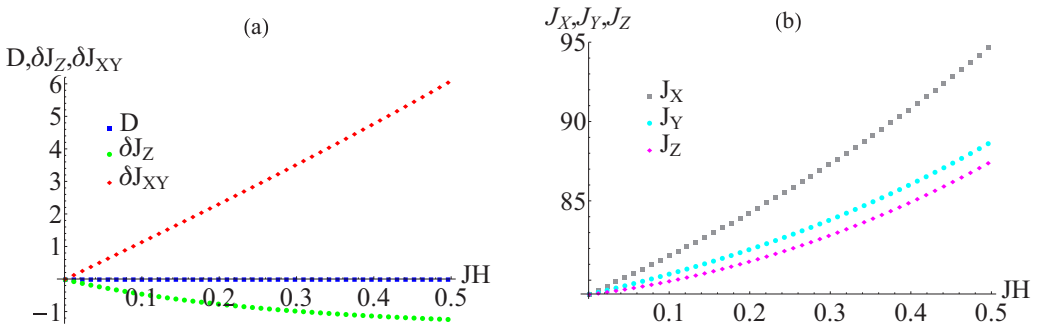

FIG. 2. (Color online) (a) Anisotropic exchange couplings $\delta J_{xy}, \delta J_z$ and the DM constant D in meV (shown by red diamond, green circle, and blue square lines, respectively) as functions of Hund's coupling, J_H. (b) The exchange couplings J_x, J_y, J_z in meV (shown by gray square, cyan circle, and magenta diamond lines, respectively) as functions of Hund's coupling, J_H. The microscopic parameters of the model are considered to be $\alpha = 0$ rad, $\Delta = 0.15$ eV, $U_2 = 1.8$ eV, $\lambda = 0.4$ eV, and $t_{\text{eff}} = 0.13$ eV.

isotropic exchange $J = J_y$. It is antiferromagnetic for all considered values of J_H and its strength varies in the range $J \in (78\text{–}95)$ meV for $J_H \in (0\text{–}0.5)$ eV. This compares well not only with an estimate $J = 51$ meV obtained by *ab initio* many-body quantum-chemical calculations [36], but also with experimental findings in Sr_2IrO_4, for which resonant inelastic x-ray scattering [5] and resonant magnetic x-ray diffuse scattering measurements [7] indicate the isotropic exchange to be $J \simeq 60$ meV and $J \simeq 100$ meV, respectively.

The effect of staggered rotations of IrO_6 octahedra. The dependencies of the anisotropic couplings $\delta J_{xy}, \delta J_z$ and D and the exchange constants J_x, J_y, J_z on the strength of the staggered rotations of the IrO_6 octahedra, α, are presented in Figs. 3(a) and 3(b). We first note that the isotropic exchange coupling $J = J_y \in (64\text{–}87)$ meV remains in good agreement with experimental estimates in the whole range of values of α considered. However, most importantly, the DM interaction becomes the dominant anisotropy even at small α. At $\alpha \simeq 0.2$ rad (11.5°), the DM interaction is already about 23 meV, which roughly corresponds to one-third of the isotropic interaction [see Fig. 3(b)]. Such a large ratio between the DM interaction and the isotropic Heisenberg exchange is very unusual and has never been observed in $3d$ transition metal oxides.

The other anisotropic interactions, both the pseudodipolar in-plane interaction, δJ_{xy}, and the Ising-like term, δJ_z, remain relatively small at finite values of α. We note that δJ_z changes sign above some angle of octahedra rotation, $\alpha_c \simeq 0.1$ rad, but, as it remains a subdominant interaction, the magnetic moments remain lying in the xy plane.

The effect of tetragonal distortion. Significant changes in the superexchange parameters are caused by the tetragonal distortion. At ambient pressure the tetragonal distortion is about $\Delta \simeq 0.1$ eV; however, larger values can be easily reached under pressure [8]. In Fig. 4(a) we plot the dependencies of the anisotropic exchange couplings $\delta J_{xy}, \delta J_z$ and the DM coupling, D, on the strength of the tetragonal distortion, Δ. An increased tetragonal distortion leads to a substantial decrease of both D and δJ_z, but the overall hierarchy of anisotropic interactions remains the same. We see that if α was not changing under pressure, the magnetic anisotropy would remain an easy plane anisotropy for all values of the tetragonal distortion.

In Fig. 4(b) we present the results on how the isotropic exchange depends on Δ at different values of α. We see that the isotropic part of the exchange coupling increases with increasing strength of the tetragonal distortion. We also see that its dependence on Δ has a quantitatively similar character for all α, with the largest values of J reached at $\alpha = 0$. Importantly, for all values of α and Δ, the isotropic

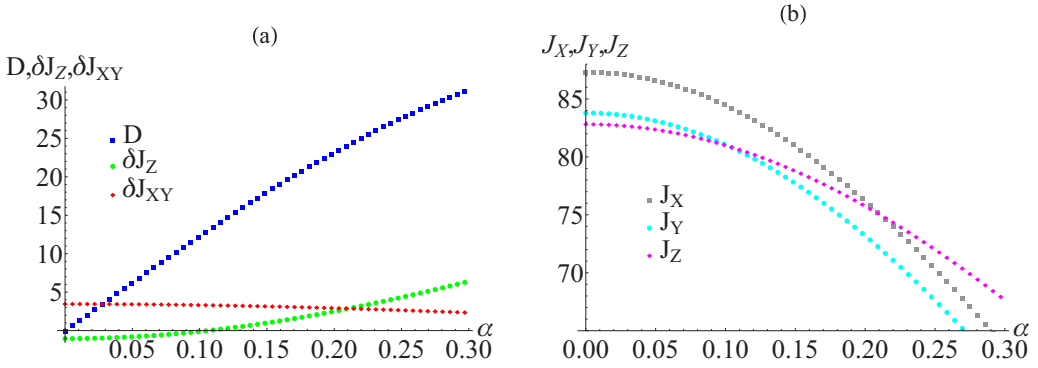

FIG. 3. (Color online) (a) Anisotropic exchange couplings $\delta J_{xy}, \delta J_z$ and DM constant D in meV (shown by red diamond, green circle, and blue square lines, respectively) and (b) the exchange couplings J_x, J_y, J_z in meV (shown by gray square, cyan circle, and magenta diamond lines, respectively) as functions of the rotation angle α. The other microscopic parameters are considered to be $\Delta = 0.15$ eV, $U_2 = 1.8$ eV, $J_H = 0.3$ eV, $\lambda = 0.4$ eV, and $t_{\text{eff}} = 0.13$ eV.

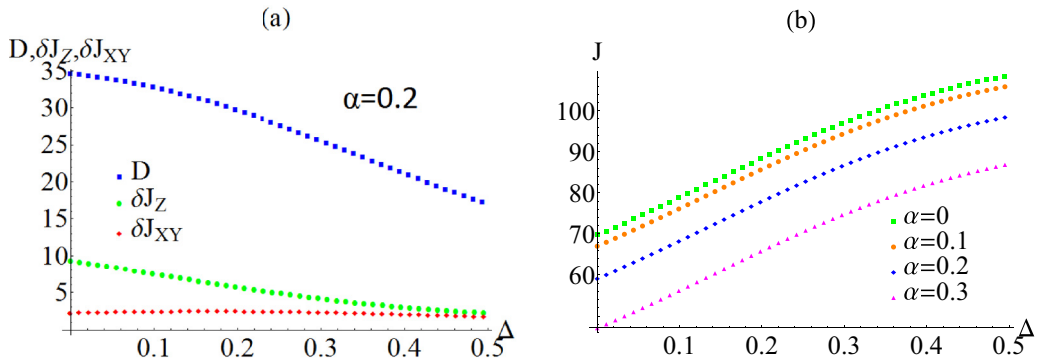

FIG. 4. (Color online) (a) Anisotropic exchange couplings δJ_{xy},δJ_z and DM constant D in meV (shown by red diamond, green circle, and blue square lines, respectively) as functions of the tetragonal CF splitting computed for $\alpha = 0.2$ rad. (b) The dependencies of the isotropic exchange J on the strength of the tetragonal CF splitting Δ. Green square, orange circle, blue diamond, and magenta triangle lines correspond to $\alpha = 0$, 0.1, 0.2, and 0.3 rad, respectively. The other parameters are $\lambda = 0.4$ eV, $U_2 = 1.8$ eV, $J_H = 0.3$ eV, and $t = 0.13$ eV.

exchange remains the dominant interaction with respect to the anisotropic terms.

Magnetic phase diagram. Finally, we compute a magnetic phase diagram of the model (33). The model allows for two distinct magnetic phases: a coplanar (or collinear) two-sublattice antiferromagnet with spins lying in the xy plane and a collinear phase with spins pointing along the c axis. The coplanar phase is characterized by a spin canting angle ϕ, which is simply given by $\phi = 1/2\ \tan^{-1}(D/J)$. The dependence of the spin canting angle ϕ (in units of α) on Δ computed for $\alpha = 0.2$ rad, corresponding to the angle of octahedral rotations at ambient pressure, and $J_H = 0.3$ is presented in Fig. 5(c). We can see that in the cubic case, $\Delta = 0$, the ratio ϕ/α is equal to unity and, therefore, spins are canted exactly like the IrO_6 octahedra. At finite Δ, the ratio ϕ/α is smaller than one, suggesting that in the presence of the tetragonal distortion the spin structure has an additional rigidity with respect to canting.

A magnetic structure can be determined by minimizing the classical energy taking into account *all* exchange couplings present in the model. Assuming that in the presence of a staggered rotation of oxygen octahedra, the magnetic structure is defined by two magnetic sublattices, A and B, and that the orientation of the magnetic moments can be described with the help of four angles, θ_A,θ_B,ϕ_A,ϕ_B, we can write the classical energy as

$$\begin{aligned} E_{\rm cl}(\theta_A,\theta_B,\phi_A,\phi_B) &= J_z \cos\theta_A \cos\theta_B \\ &+ \frac{(J_x + J_y)}{2} \sin\theta_A \sin\theta_B(\cos\phi_A \cos\phi_B + \sin\phi_A \sin\phi_B) \\ &- D\ \sin\theta_A \sin\theta_B(\cos\phi_A \sin\phi_B - \sin\phi_A \cos\phi_B). \end{aligned} \quad (36)$$

One can easily check that the contribution of the pseudodipolar interaction to the classical energy cancels out. Thus, for any set of microscopic parameters, the classical ground state is determined by the competition between the DM interaction and the Ising-like anisotropy in the presence of a dominating AFM isotropic exchange.

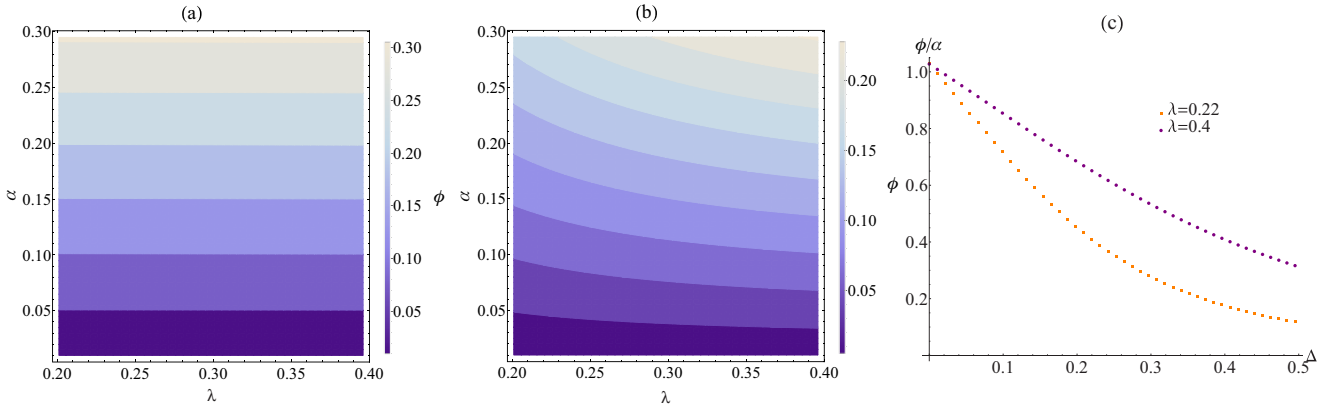

FIG. 5. (Color online) Mean field magnetic phase diagram in the parameter space of rotation angle α and the SOC coupling λ computed (a) in the absence of the tetragonal distortion, $\Delta = 0$, eV and (b) in the presence of the tetragonal distortion, $\Delta = 0.15$ eV. In both parameter sets, the obtained magnetic structure is coplanar antiferromagnet with varying spin canting angle $\phi = [\pi - (\phi_A - \phi_B)]/2$, where ϕ_A and ϕ_B are the polar angles of spins on sublattices A and B. The color on the plots indicates the scale for which the angle ϕ changes with dark blue being the smallest and gray being the highest value of the angle ϕ. The canted spin order is stabilized by a staggered rotation of oxygen tetrahedra in the presence of the SOC. (c) The dependence of the spin canting angle $\phi = 1/2\ \tan^{-1}(D/J)$ (in units of α) on the strength of the tetragonal CF splitting Δ computed for $\lambda = 0.22$ eV (orange square line) and $\lambda = 0.4$ eV (purple circle line). The other microscopic parameters are chosen to be $U_2 = 1.8$ eV, $J_H = 0.3$ eV, $t_{\rm eff} = 0.13$ eV, and $\alpha = 0.2$ rad.

In Figs. 5(a) and 5(b) we present a mean field magnetic phase diagram, where for each set of parameters the magnetic structure is determined by minimizing $E_{\rm cl}$ with respect to $\theta_A,\theta_B,\phi_A,\phi_B$. We considered two cases: Fig. 5(a) displays a phase diagram computed in the absence of tetragonal distortion ($\Delta = 0$ eV) and Fig. 5(b) displays a phase diagram computed in the presence of the tetragonal distortion ($\Delta = 0.15$ eV). In both cases we considered the Hund's coupling to be equal to $J_H = 0.3$ eV. Both phase diagrams contain only the coplanar antiferromagnet with varying canting angle $\phi = [\pi - (\phi_A - \phi_B)]/2$, where ϕ_A and ϕ_B are polar angles of spins on sublattices A and B. The color on the plots indicates the magnitude scale of the angle ϕ: dark blue colors correspond to the smallest and light gray colors correspond to the highest values of the angle ϕ. As we discussed above, in the absence of the tetragonal distortion, the canting of magnetic moments rigidly follows the octahedral rotation and the canting angle ϕ is exactly equal to the rotation angle α for all values of the SOC strength [see Fig. 5(a)]. However, once the tetragonal distortion is present, the canting angle ϕ becomes smaller than α. Moreover, the ratio ϕ/α decreases with decrease of the SOC constant [see Fig. 5(b)].

We have to note that our findings are not in full agreement with the phase diagram presented by Jackeli and Khalliulin in Ref. [11], which shows that at large values of tetragonal distortion the spin-flop transition from the in-plane canted spin state happens to a collinear antiferromagnetic order along the z axis. Instead, we found that at the considered set of parameters the tetragonal distortion may lead to a disappearance of the ferromagnetic moment and a stabilization of the antiferromagnetic order in the easy xy plane.

Our findings are, however, in qualitative agreement with both pressure experiments in Sr_2IrO_4 [8] and the x-ray resonant magnetic scattering study comparing the magnetic and electronic structures of Sr_2IrO_4 and Ba_2IrO_4 [9]. The first study shows that when the tetragonal distortion due to pressure becomes relatively strong, about 17 GPa, the ferromagnetic order disappears. This magnetic transition was not attributed to the gradual disappearance of the IrO_6 rotations under pressure, because it would have likely resulted in some kind of structural transition which was not observed. They also found that the application of pressure up to at least 40 GPa does neither destroy the insulating behavior nor, probably, the antiferromagnetic order. However, the direction of the antiferromagnetic order parameter was not determined. The second study shows the general robustness of the basal-plane antiferromagnetic order in single-layer iridates. They found that, in both Sr_2IrO_4 and Ba_2IrO_4, the antiferromagnetic component is oriented along the [110] direction despite the fact that moving from Sr_2IrO_4 to Ba_2IrO_4 the tetragonal distortion is nearly doubled.

B. Application to $Sr_2Ir_{1-x}Rh_xO_4$

In this section we take a look at the properties of the $Sr_2Ir_{1-x}Rh_xO_4$ family of compounds, which results from substituting Sr_2IrO_4 by Rh ions [34]. Doping iridates with Rh ions does not change the band filling since Rh and Ir are in the same family of elements. However, the $4d$ orbitals of Rh are smaller than the $5d$ orbitals of Ir, which leads to a higher Coulomb repulsion, Hund's coupling, and tetragonal CF splitting. Smaller atoms (such as Rh) also have reduced relativistic effects, including SO coupling. The effective hopping is reduced both due to a smaller overlap of the less extended $4d$ orbitals as well as due to the increased Coulomb repulsion. All of this increases the importance of correlation effects and CF splitting as compared to that of SOC.

We also note that Sr_2RhO_4, the limiting case of Rh doping, shares with Sr_2IrO_4 the structural feature of staggered octahedra rotations about the axis perpendicular to the Rh/Ir planes. The angles of rotation are similar to each other: $\sim 9.4^\circ$ for Sr_2RhO_4 and $\sim 12^\circ$ for Sr_2IrO_4 [34]. This structure is preserved at intermediate levels of doping. As a result in the doped compounds the same interaction components are present as in pure Sr_2IrO_4 (Coulomb, Hund, SOC, CF, oxygen-assisted hopping, and lattice distortions). Thus we expect the magnetic Hamiltonian to have the same structure of interactions. What changes is the overall energy balance of on-site interactions, which in the Rh-doped iridates eventually leads to the appearance of different magnetic phases compared to those in pure iridium compounds.

Let us note that a reduced hopping simply leads to a decrease of the energy scale of all interactions (both the isotropic term and the anisotropies). The effects of reduced SOC are more intricate since SOC is the only interaction that mixes the orbital and the spin degrees of freedom of the holes. Thus we also expect the energy scale of the anisotropies to be reduced as compared to the isotropic term. This, however, does not diminish the importance of the anisotropic terms as their essential role is to break the SU(2) symmetry of the isotropic interaction.

In Figs. 6(a) and 6(c) we plot the dependencies of the anisotropic and isotropic interactions, respectively, on the strength of λ. We adjust all other parameters in accordance with the rhodium doping picture discussed above: $\Delta = 0.2$ eV, $\alpha = 0.2$ rad, $J_H = 0.5$ eV, $U_2 = 2.5$ eV, and $t_{\rm eff} = 0.1$ eV. A similar set of parameters might be realized at low Rh doping. As expected, the overall energy scale of the magnetic interactions is decreased due to Coulomb repulsion and smaller hopping. In Fig. 6(a) we also see that once the SOC becomes too small relative to other interactions to effectively mix the orbital and spin degrees of freedom the anisotropic interactions quickly drop and reach zero in the limit of no SOC.

The behavior of the isotropic interaction is more interesting as it is weakly nonmonotonic as a function of SO coupling. This can be explained when we look at different values of Δ. Gray, cyan, and magenta lines in Fig. 6(c) show the isotropic interaction corresponding to $\Delta = 0.1$, 0.2, and 0.3 eV, respectively. Since cubic orbitals have different hopping amplitudes due to the staggered rotations of the octahedra and the orbital symmetries (see Appendix B), the orbital composition of the ground state also determines the isotropic part of the exchange Hamiltonian. As the orbital composition is very sensitive to the interplay between the SOC and the CF, the small changes in their relative contribution lead to a nonmonotonic behavior of J.

Figure 6(b) shows the dependence of the DM anisotropy on the staggered rotation angle α computed for $\lambda = 0.2$, 0.3, and 0.4 eV (respectively, black, cyan, and blue lines). As is

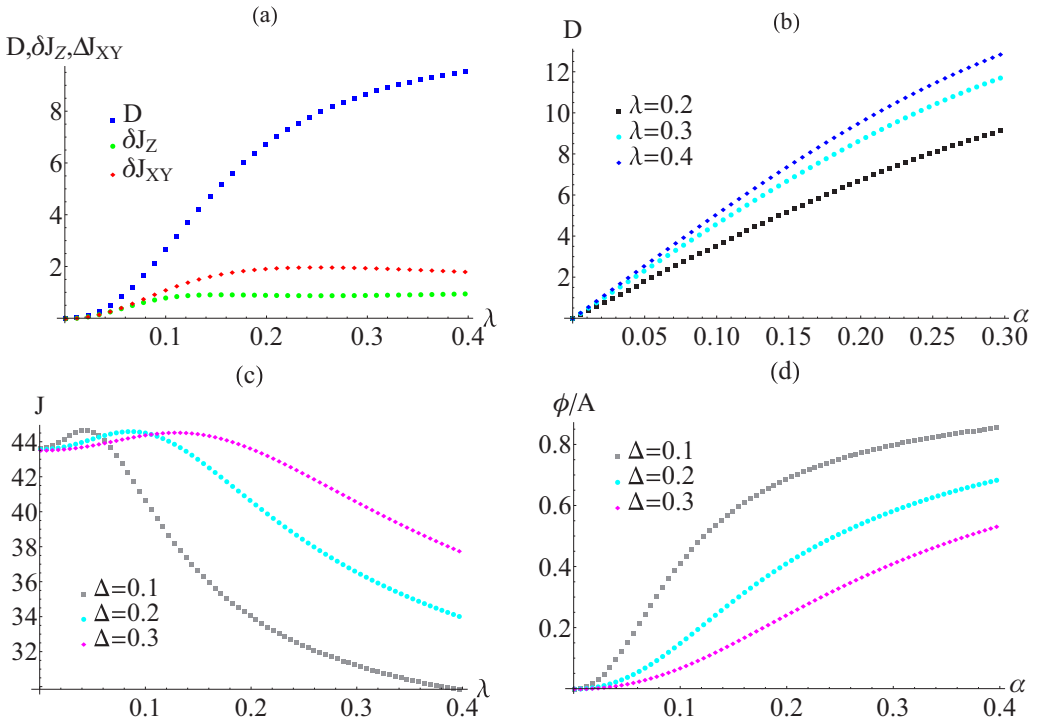

FIG. 6. (Color online) (a) Anisotropic exchange couplings δJ_{xy},δJ_z and the DM constant D (in meV) as functions of SOC constant λ shown by red diamond, green circle, and blue square lines, respectively. (b) The DM constant D (in meV) as function of rotation angle α. Black square, cyan circle, and blue diamond lines correspond to $\lambda = 0.2$, 0.3, and 0.4 eV, respectively. (a),(b) The tetragonal field is considered to be equal to $\Delta = 0.2$ eV. (c) The isotropic exchange J (in meV) and (d) the spin canting angle ϕ (in units of α) as functions of SOC constant λ. Gray square, cyan circle, and magenta diamond lines correspond to $\Delta = 0.1$, 0.2, and 0.3 eV, respectively. (a),(c),(d) The rotation angle is considered to be equal to $\alpha = 0.2$ rad. The remaining parameters are $J_H = 0.5$ eV, $U_2 = 2.5$ eV, and $t_{\text{eff}} = 0.1$ eV.

the case for the pure Sr_2IrO_4 compound the DM interaction depends heavily on the angle but, as we discussed above, the overall range of DM interactions is smaller.

Finally, in Fig. 6(d) we present the spin canting angle ϕ (in units of α) as a function of the SOC constant λ for various values of the tetragonal distortion Δ. As expected, the canting angle is zero in the limit of zero SOC and is increasing with increasing λ, demonstrating the key role of SOC in the entanglement of the spin and lattice degrees of freedom. As we discussed above, the spin canting angle is suppressed by the tetragonal distortion.

Our findings are in a qualitative agreement with experimental findings for the $Sr_2Ir_{1-x}Rh_xO_4$ family of compounds showing that Rh doping rapidly suppresses the magnetic transition temperature T_C from 240 K at $x = 0$ to almost zero at $x = 0.16$ [34]. The disappearance of long range magnetic order at small doping in real compounds is a rather complicated phenomenon, related to both the reduction of magnetic interactions but also to the more metallic behavior of doped compounds. This aspect, however, cannot be considered in our approach based on the assumption of a Mott insulator. We can only speculate that in Rh-doped iridates the splitting between the $\mathbf{J} = 1/2$ and the $\mathbf{J} = 3/2$ states is substantially smaller than in pure iridium systems and, consequently, these two manifolds are strongly mixed by both Hund's coupling and tetragonal CF. The latter leads to a wider bandwidth and more metallic behavior. Interestingly, at high Rh doping, the system again becomes insulating, however for rather different reasons. There is an energy level mismatch for the Rh and Ir sites that makes the hopping of the carriers between Rh and Ir ions more difficult. The randomness of the Rh/Ir occupations gives rise to Anderson localization and an insulating state [34]. The magnetically ordered phase reappeared at $x > 0.4$, but because of frustration it has rather low ordering temperature T_C of the order half a kelvin. This magnetic phase needs to be studied in detail both experimentally and theoretically.

V. CONCLUSION

In this paper we provided a theoretical framework for the derivation of the effective superexchange Hamiltonian governing magnetic properties of transition metal oxides with partially filled $4d$ and $5d$ shells. We particularly focused on iridates and rhodates—materials which exhibit a rich variety of behavior owing to the interplay of correlation effects, strong SOC, and lattice distortions. Our approach allows one to relate the nontrivial magnetic behavior observed in these materials to their microscopic parameters. We show that the pseudospin superexchange interactions governing the magnetic properties of this class of insulating materials have anisotropic components of unusual types, leading not only to a dimensional reduction in pseudospin space (i.e., easy plane or easy axis anisotropy), but also to the chiral DM interaction and to additional frustration by bond-dependent interactions.

How to derive exchange couplings from a given Hubbard-type Hamiltonian in the Mott-insulating regime is generally

well understood. What gives rise to a certain complexity in our case is the combination of interactions and single-particle energy shifts operating in different Hilbert subspaces. We restrict our consideration to the case of a ground state configuration of a single hole per transition metal ion in a pseudospin doublet state in one of the d-orbital multiplets. The exchange process then involves intermediate states with either zero holes or two holes. The latter states are governed by the Coulomb interaction components, especially the Hund's coupling. These ionic eigenstates need to be constructed and must be projected onto the single-particle states describing the hopping processes. The resulting exchange couplings are then given by summation over all relevant intermediate eigenstates of the corresponding hopping element squared over the excitation energy of the intermediate state.

The proposed theoretical approach can be applied to compute exchange couplings in iridium and rhodium oxides with different lattice geometries. Many of these systems have been suggested as candidates for either interesting magnetic orders or spin-liquid behavior in the Mott insulator regime. Although the approach is quite general and can be applied to a variety of compounds, in this paper we focused on the single-layer Sr_2IrO_4 and $Sr_2Ir_{1-x}Rh_xO_4$ compounds, which have received much attention recently. For these systems we first derive the isotropic and anisotropic interactions analytically and then study their dependencies on microscopic parameters such as Hund's and SOC coupling, and the strength of the lattice distortions.

Our results are the following. First, the overall strengths of the exchange couplings calculated by us appear to be in good agreement with experimental data, where available. While the Ising-like and pseudospin anisotropic interactions are typically not larger than 10% of the isotropic exchange, the DM coupling is unusually large. It may be as large as 50% of the isotropic exchange coupling for realistic values of the octahedra rotation angle. This emphasizes the importance of the SOC.

We computed the magnetic phase diagram of the model in the approximation of treating the pseudospins as classical objects. We show that for the parameter set most closely corresponding to the actual microscopic parameters of Sr_2IrO_4, the magnetic ground state of this compound is a coplanar canted antiferromagnet. This finding is in agreement with the experimental observation of the weak ferromagnetic moment accompanying the ground-state antiferromagnetic order in Sr_2IrO_4. We computed the spin canting angle and show that its magnitude scales with the angle of the staggered rotations of the IrO_6 octahedra, as observed experimentally.

Finally, we studied how the properties of the pure iridium systems are changed with Rh doping. We show that Rh doping significantly modifies the hierarchy of many-body and single-particle interactions: the weaker SOC combined with a stronger Coulomb interaction on Rh sites lead to overall smaller magnetic interactions and a weaker coupling between magnetic and structural degrees of freedom.

ACKNOWLEDGMENTS

We thank G. Jackeli and G.-W. Chern for useful discussions. N.P. and Y.S. acknowledge the support from NSF Grant No. DMR-1255544. N.P. is also grateful for the hospitality of the visitors program at MPIPKS, where a part of the work on this manuscript has been done. P.W. thanks the Department of Physics at the University of Wisconsin-Madison for hospitality during a stay as a visiting professor and acknowledges an ICAM senior scientist fellowship. P.W. also acknowledges partial support through the DFG research unit "Quantum phase transitions."

APPENDIX A: STRUCTURE OF THE HAMILTONIAN MATRIX (14)

The block structure of the Hamiltonian matrix has the following form. States $|\mathcal{J},1\rangle$ and $|\mathcal{J},10\rangle$ form the first block. The eigenstates are

$$\begin{aligned} |D,1\rangle &= c_{1,1}|\mathcal{J},1\rangle + c_{1,10}|\mathcal{J},10\rangle, \\ |D,10\rangle &= c_{10,1}|\mathcal{J},1\rangle + c_{10,10}|\mathcal{J},10\rangle, \end{aligned} \tag{A1}$$

where $c_{1,1}$, $c_{1,10}$, $c_{10,1}$, and $c_{10,10}$ are the components of eigenvectors which are obtained by diagonalizing (14). We denote the eigenvalues of this block as E_1 and E_{10}.

The second block involves states $|\mathcal{J},8\rangle$ and $|\mathcal{J},15\rangle$. The Hamiltonian matrix for (8,15) is identical to the one for (1,10). Therefore,

$$\begin{aligned} |D,8\rangle &= c_{8,8}|\mathcal{J},8\rangle + c_{8,15}|\mathcal{J},15\rangle, \\ |D,15\rangle &= c_{15,8}|\mathcal{J},8\rangle + c_{15,15}|\mathcal{J},15\rangle, \end{aligned} \tag{A2}$$

with $c_{8,8} = c_{1,1}, c_{15,15} = c_{10,10}, c_{8,15} = c_{1,10}$, and $c_{15,8} = c_{10,1}$. The eigenenergies of this block are simply $E_8 = E_1$ and $E_{15} = E_{10}$.

The third block involves the three states $|\mathcal{J},2\rangle$, $|\mathcal{J},3\rangle$, and $|\mathcal{J},11\rangle$. The eigenstates are given by

$$\begin{aligned} |D,2\rangle &= c_{2,2}|\mathcal{J},2\rangle + c_{2,3}|\mathcal{J},3\rangle + c_{2,11}|\mathcal{J},11\rangle, \\ |D,3\rangle &= c_{3,2}|\mathcal{J},2\rangle + c_{3,3}|\mathcal{J},3\rangle + c_{3,11}|\mathcal{J},11\rangle, \\ |D,11\rangle &= c_{11,2}|\mathcal{J},2\rangle + c_{11,3}|\mathcal{J},3\rangle + c_{11,11}|\mathcal{J},11\rangle, \end{aligned} \tag{A3}$$

and eigenvalues are E_2, E_3, and E_{11}.

The fourth block consists of (7,6,14) states and is equivalent to the (2,3,11) block. The eigenstates are given by

$$\begin{aligned} |D,7\rangle &= c_{7,7}|\mathcal{J},7\rangle + c_{7,6}|\mathcal{J},6\rangle + c_{7,14}|\mathcal{J},14\rangle, \\ |D,6\rangle &= c_{6,7}|\mathcal{J},7\rangle + c_{6,6}|\mathcal{J},6\rangle + c_{6,14}|\mathcal{J},14\rangle, \\ |D,14\rangle &= c_{14,7}|\mathcal{J},7\rangle + c_{14,6}|\mathcal{J},6\rangle + c_{14,14}|\mathcal{J},14\rangle. \end{aligned} \tag{A4}$$

The fifth block consists of (4,5,9,12,13) states. The eigenstates are given by

$$\begin{aligned} |D,4\rangle &= c_{4,4}\,|\mathcal{J},4\rangle + c_{4,5}\,|\mathcal{J},5\rangle + c_{4,9}\,|\mathcal{J},9\rangle + c_{4,12}\,|\mathcal{J},12\rangle + c_{4,13}\,|\mathcal{J},13\rangle\,, \\ |D,5\rangle &= c_{5,4}\,|\mathcal{J},4\rangle + c_{5,5}\,|\mathcal{J},5\rangle + c_{5,9}\,|\mathcal{J},9\rangle + c_{5,12}\,|\mathcal{J},12\rangle + c_{5,13}\,|\mathcal{J},13\rangle\,, \\ |D,9\rangle &= c_{9,4}\,|\mathcal{J},4\rangle + c_{9,5}\,|\mathcal{J},5\rangle + c_{9,9}\,|\mathcal{J},9\rangle + c_{9,12}\,|\mathcal{J},12\rangle + c_{9,13}\,|\mathcal{J},13\rangle\,, \end{aligned}$$

$$|D,12\rangle = c_{12,4}\,|\mathcal{J},4\rangle + c_{12,5}\,|\mathcal{J},5\rangle + c_{12,9}\,|\mathcal{J},9\rangle + c_{12,12}\,|\mathcal{J},12\rangle + c_{12,13}\,|\mathcal{J},13\rangle\,,$$
$$|D,13\rangle = c_{13,4}\,|\mathcal{J},4\rangle + c_{13,5}\,|\mathcal{J},5\rangle + c_{13,9}\,|\mathcal{J},9\rangle + c_{13,12}\,|\mathcal{J},12\rangle + c_{13,13}\,|\mathcal{J},13\rangle\,. \quad \text{(A5)}$$

Note that the same block structure survives in the presence of the lattice distortions.

APPENDIX B: HOPPING OPERATOR FOR 180° Ir-O-Ir BOND

We first consider the hopping operator on the square lattice in the simplest case with no tetragonal distortion, $\Delta = 0$, and no rotations of the IrO_6 octahedra. Without loss of generality we consider x bonds, and then using symmetry arguments we obtain transfer matrix elements along y bonds. Along an x bond the hopping occurs either through p_y or p_z orbitals of oxygen. The p_y orbital overlaps with $|Z\rangle = |xy\rangle$ and p_z orbital overlaps with $|Y\rangle = |zx\rangle$ orbitals of iridium. Correspondingly, we denote the hopping amplitudes as $t_{Z,y}$ and $t_{Y,z}$. However, on the undistorted lattice $t_{Z,y} = t_{Y,z}$ and to simplify notations we denote the hopping amplitude as t. Integrating over the oxygen ions, the effective hopping between Ir ions can be approximated as $t_{\rm eff} = t^2/\Delta_{pd}$, where Δ_{pd} is the charge-transfer gap. In our calculations we consider $t_{\rm eff} = 0.13$ eV. The effective hopping Hamiltonian between Ir ions along the x bond is then given by

$$H_t^x = t_{\rm eff} \sum_n \left(a^\dagger_{Z\sigma,n} a_{Z\sigma,n+x} + a^\dagger_{Y\sigma,n} a_{Y\sigma,n+x} + \text{H.c.}\right). \quad \text{(B1)}$$

Expressing operators $a^\dagger_{Z\sigma,n}$, etc., in terms of $b^\dagger_{\gamma,n}$ operators, we get

$$H_t^x = \sum_n \sum_{\gamma,\gamma'} T^{\gamma,\gamma'}_{n,n+x} (b^\dagger_{n,\gamma} b_{n+x,\gamma'} + \text{H.c.}), \quad \text{(B2)}$$

where the elements of the effective transfer matrix, $T^{\gamma,\gamma'}_{n,n+x}$, between γ and γ' orbitals can be written as

$$T^{\gamma,\gamma'}_{n,n+x} = t_{\rm eff}\left(\tau_Z^{\gamma,\gamma'} + \tau_Y^{\gamma,\gamma'}\right). \quad \text{(B3)}$$

Here we use the following notation:

$$\tau_Z^{\gamma,\gamma'} = {}_{\gamma'}\langle J, J_z|\hat{T}|p^y_\sigma\rangle\langle p^y_\sigma|\hat{T}|J, J_z\rangle_\gamma,$$
$$\tau_Y^{\gamma,\gamma'} = {}_{\gamma'}\langle J, J_z|\hat{T}|p^z_\sigma\rangle\langle p^z_\sigma|\hat{T}|J, J_z\rangle_\gamma, \quad \text{(B4)}$$

where $\hat{T}$ are hopping operators connecting neighboring Ir and O orbitals. In matrix form τ_Z, τ_Y are given by

$$\hat{\tau}_Z = \frac{1}{3}\begin{pmatrix} 1 & 0 & 0 & -\sqrt{2} & 0 & 0 \\ 0 & 1 & 0 & 0 & \sqrt{2} & 0 \\ 0 & 0 & 0 & 0 & 0 & 0 \\ -\sqrt{2} & 0 & 0 & 2 & 0 & 0 \\ 0 & \sqrt{2} & 0 & 0 & 2 & 0 \\ 0 & 0 & 0 & 0 & 0 & 0 \end{pmatrix} \quad \text{(B5)}$$

and

$$\hat{\tau}_Y = \frac{1}{6}\begin{pmatrix} 2 & 0 & 0 & \sqrt{2} & 0 & -\sqrt{6} \\ 0 & 2 & \sqrt{6} & 0 & -\sqrt{2} & 0 \\ 0 & \sqrt{6} & 3 & 0 & -\sqrt{3} & 0 \\ \sqrt{2} & 0 & 0 & 1 & 0 & -\sqrt{3} \\ 0 & -\sqrt{2} & -\sqrt{3} & 0 & 1 & 0 \\ -\sqrt{6} & 0 & 0 & -\sqrt{3} & 0 & 3 \end{pmatrix}. \quad \text{(B6)}$$

In the presence of tetragonal distortion and octahedra rotations, as in the case of Sr_2IrO_4, the transfer matrix elements are more conveniently described using the global coordinate system. The hopping between γ and γ' states is then given by

$$\bar{T}^{\gamma,\gamma'}_{n,n+x} = t_{\rm eff}\left(\bar{\tau}_Z^{\gamma,\gamma'} + \bar{\tau}_Y^{\gamma,\gamma'}\right), \quad \text{(B7)}$$

where modified transfer matrices are defined as

$$\bar{\tau}_Z^{\gamma,\gamma'} = {}_{\gamma'}\langle\Psi_B|\hat{T}|p^y_\sigma\rangle\langle p^y_\sigma|\hat{T}|\Psi_A\rangle_\gamma, \quad \text{(B8)}$$
$$\bar{\tau}_Y^{\gamma,\gamma'} = {}_{\gamma'}\langle\Psi_B|\hat{T}|p^z_\sigma\rangle\langle p^z_\sigma|\hat{T}|\Psi_A\rangle_\gamma.$$

Explicitly, $\hat{\bar{\tau}}_Z$ and $\hat{\bar{\tau}}_Y$ are given by

$$\hat{\bar{\tau}}_Z = c_\alpha^2\begin{pmatrix} s_\theta^2 & 0 & 0 & s_\theta c_\theta & 0 & 0 \\ 0 & s_\theta^2 & 0 & 0 & s_\theta c_\theta & 0 \\ 0 & 0 & 0 & 0 & 0 & 0 \\ s_\theta c_\theta & 0 & 0 & c_\theta^2 & 0 & 0 \\ 0 & s_\theta c_\theta & 0 & 0 & c_\theta^2 & 0 \\ 0 & 0 & 0 & 0 & 0 & 0 \end{pmatrix} \quad \text{(B9)}$$

and

$$\hat{\bar{\tau}}_Y = \frac{1}{2}\begin{pmatrix} c_\theta^2 e^{2\imath\alpha} & 0 & 0 & -s_\theta c_\theta & 0 & c_\theta e^{2\imath\alpha} \\ 0 & c_\theta^2 e^{-2\imath\alpha} & -c_\theta e^{-2\imath\alpha} & 0 & -s_\theta c_\theta & 0 \\ 0 & -c_\theta e^{-2\imath\alpha} & e^{2\imath\alpha} & 0 & s_\theta & 0 \\ -s_\theta c_\theta & 0 & 0 & s_\theta^2 e^{2\imath\alpha} & 0 & -s_\theta \\ 0 & -s_\theta c_\theta & s_\theta & 0 & s_\theta^2 e^{-2\imath\alpha} & 0 \\ c_\theta e^{-2\imath\alpha} & 0 & 0 & -s_\theta & 0 & e^{-2\imath\alpha} \end{pmatrix}. \quad \text{(B10)}$$

[1] G. Cao, J. Bolivar, S. McCall, J. E. Crow, and R. P. Guertin, Phys. Rev. B **57**, R11039 (1998).

[2] B. J. Kim, H. Jin, S. J. Moon, J.-Y. Kim, B.-G. Park, C. S. Leem, J. Yu, T. W. Noh, C. Kim, S.-J. Oh, J.-H. Park, V. Durairaj, G. Cao, and E. Rotenberg, Phys. Rev. Lett. **101**, 076402 (2008).

[3] S. J. Moon, H. Jin, W. S. Choi, J. S. Lee, S. S. A. Seo, J. Yu, G. Cao, T. W. Noh, and Y. S. Lee, Phys. Rev. B **80**, 195110 (2009).

[4] B. J. Kim, H. Ohsumi, T. Komesu, S. Sakai, T. Morita, H. Takagi, and T. Arima, Science **323**, 1329 (2009).

[5] J. Kim, D. Casa, M. H. Upton, T. Gog, Y.-J. Kim, J. F. Mitchell, M. van Veenendaal, M. Daghofer, J. van den Brink, G. Khaliullin, and B. J. Kim, Phys. Rev. Lett. **108**, 177003 (2012).
[6] J. W. Kim, Y. Choi, J. Kim, J. F. Mitchell, G. Jackeli, M. Daghofer, J. van den Brink, G. Khaliullin, and B. J. Kim, Phys. Rev. Lett. **109**, 037204 (2012).
[7] S. Fujiyama, H. Ohsumi, T. Komesu, J. Matsuno, B. J. Kim, M. Takata, T. Arima, and H. Takagi, Phys. Rev. Lett. **108**, 247212 (2012).
[8] D. Haskel, G. Fabbris, M. Zhernenkov, P. P. Kong, C. Q. Jin, G. Cao, and M. van Veenendaal, Phys. Rev. Lett. **109**, 027204 (2012).
[9] S. Boseggia, R. Springell, H. C. Walker, H. M. Ronnow, Ch. Ruegg, H. Okabe, M. Isobe, R. S. Perry, S. P. Collins, and D. F. McMorrow, Phys. Rev. Lett. **110**, 117207 (2013).
[10] M. F. Cetin, P. Lemmens, V. Gnezdilov, D. Wulferding, D. Menzel, T. Takayama, K. Ohashi, and H. Takagi, Phys. Rev. B **85**, 195148 (2012).
[11] G. Jackeli and G. Khaliullin, Phys. Rev. Lett. **102**, 017205 (2009).
[12] F. Wang and T. Senthil, Phys. Rev. Lett. **106**, 136402 (2011).
[13] C. Martins, M. Aichhorn, L. Vaugier, and S. Biermann, Phys. Rev. Lett. **107**, 266404 (2011).
[14] B. H. Kim, G. Khaliullin, and B. I. Min, Phys. Rev. Lett. **109**, 167205 (2012).
[15] R. Arita, J. Kunes, A. V. Kozhevnikov, A. G. Eguiluz, and M. Imada, Phys. Rev. Lett. **108**, 086403 (2012).
[16] Y. Okamoto, M. Nohara, H. Aruga-Katori, and H. Takagi, Phys. Rev. Lett. **99**, 137207 (2007).
[17] M. J. Lawler, H.-Y. Kee, Y. B. Kim, and A. Vishwanath, Phys. Rev. Lett. **100**, 227201 (2008).
[18] S. Nakatsuji, Y. Machida, Y. Maeno, T. Tayama, T. Sakakibara, J. van Duijn, L. Balicas, J. N. Millican, R. T. Macaluso, and J. Y. Chan, Phys. Rev. Lett. **96**, 087204 (2006).
[19] Y. Machida, S. Nakatsuji, Y. Maeno, T. Tayama, T. Sakakibara, and S. Onoda, Phys. Rev. Lett. **98**, 057203 (2007).
[20] Y. Machida, Satoru, S. Onoda, T. Tayama, and T. Sakakibara, Nature (London) **463**, 210 (2010).
[21] D. Pesin and L. Balents, Nat. Phys. **6**, 376 (2010).
[22] B.-J. Yang and Y. B. Kim, Phys. Rev. B **82**, 085111 (2010).
[23] E. K.-H. Lee, S. Bhattacharjee, and Y. B. Kim, Phys. Rev. B **87**, 214416 (2013).
[24] S. Zhao, J. M. Mackie, D. E. MacLaughlin, O. O. Bernal, J. J. Ishikawa, Y. Ohta, and S. Nakatsuji, Phys. Rev. B **83**, 180402(R) (2011); J. Phys. Soc. Jpn. **81**, 034709 (2012).
[25] J. J. Ishikawa, E. C. T. O'Farrell, and S. Nakatsuji, Phys. Rev. B **85**, 245109 (2012).
[26] A. Shitade, H. Katsura, J. Kunes, X.-L. Qi, S.-C. Zhang, and N. Nagaosa, Phys. Rev. Lett. **102**, 256403 (2009).
[27] J. Chaloupka, G. Jackeli, and G. Khaliullin, Phys. Rev. Lett. **105**, 027204 (2010).
[28] Y. Singh and P. Gegenwart, Phys. Rev. B **82**, 064412 (2010).
[29] Y. Singh, S. Manni, J. Reuther, T. Berlijn, R. Thomale, W. Ku, S. Trebst, and P. Gegenwart, Phys. Rev. Lett. **108**, 127203 (2012).
[30] X. Liu, T. Berlijn, W.-G. Yin, W. Ku, A. Tsvelik, Y.-J. Kim, H. Gretarsson, Y. Singh, P. Gegenwart, and J. P. Hill, Phys. Rev. B **83**, 220403 (2011).
[31] F. Ye, S. Chi, H. Cao, B. C. Chakoumakos, J. A. Fernandez-Baca, R. Custelcean, T. F. Qi, O. B. Korneta, and G. Cao, Phys. Rev. B **85**, 180403 (2012).
[32] C. C. Price and N. B. Perkins, Phys. Rev. Lett. **109**, 187201 (2012).
[33] C. C. Price and N. B. Perkins, Phys. Rev. B **88**, 024410 (2013).
[34] T. F. Qi, O. B. Korneta, L. Li, K. Butrouna, V. S. Cao, X. Wan, P. Schlottmann, R. K. Kaul, and G. Cao, Phys. Rev. B **86**, 125105 (2012).
[35] Y. Luo, C. Cao, B. Si, Y. Li, J. Bao, H. Guo, X. Yang, C. Shen, C. Feng, J. Dai, G. Cao, and Z.-a. Xu, Phys. Rev. B **87**, 161121 (2013).
[36] V. M. Katukuri, H. Stoll, J. van den Brink, and L. Hozoi, Phys. Rev. B **85**, 220402 (2012).